

Supporting Information

Rational design of donor-acceptor structure in covalent heptazine frameworks to boost photocatalytic nitrogen fixation

Yuhang Deng^a, Tao Sun^a, Shi Zhou^c, Wei Jiang^{a,b,*}, Chunbo Liu^{a,c}, Chunhong Ma^{a,c,*},

Guangbo Che^{d,*}

Table of Contents

Experimental Details

Chemicals and reagents

Materials characterizations

Synthesis of g-C₃N₄

Synthesis of C₆N₇Cl₃

Synthesis of catalyst

DFT calculation method

Performance measurement

Results and Discussion

Fig.S1 The XRD of TAPT-CTF, TAPB-CHF, and TAPT-CHF.

Fig.S2 The FT-IR of TAPB-CHF and TAPT-CTF.

Fig.S3 The ¹³C NMR of TAPB-CHF and TAPT-CTF.

Fig.S4 The (a) survey, (b) C 1s and, (c) N 1s spectra of TAPT-CHF.

Fig.S5 (a-c) SEM, (d-f) TEM and (g-i) EDS of TAPB-CHF, TAPT-CHF and TAPT-CTF.

Fig.S6 The N₂ sorption isotherms of TAPT-CTF, TAPB-CHF, and TAPT-CHF.

Fig.S7 The pore size distribution curve of TAPT-CTF, TAPB-CHF, and TAPT-CHF.

Fig.S8 The contact angle test of TAPT-CTF, TAPB-CHF, and TAPT-CHF.

Fig.S9 The bandgap of TAPB-CHF.

Fig.S10 The bandgap of TAPT-CHF.

Fig.S11 The bandgap of TAPT-CTF.

Fig.S12 Mott–Schottky plots of TAPB-CHF.

Fig.S13 Mott–Schottky plots of TAPT-CHF.

Fig.S14 Mott–Schottky plots of TAPT-CTF.

Fig.S15 The band diagram of TAPB-CHF, TAPT-CHF, and TAPT-CTF.

Fig.S16 The PL of TAPB-CHF, TAPT-CHF, TAPT-CTF and H₂PtCl₆.

Fig.S17 The LSV of TAPB-CHF, TAPT-CHF and TAPT-CTF.

Fig.S18 The standard curve of NH₃ measured by Nessler reagent spectrophotometry.

Fig.S19 NH₃ evolution curves.

Fig.S20 Comparative analysis among peers.

Fig.S21 NH₃ evolution curve without H₂PtCl₆ aqueous solution.

Fig.S22 NH₃ evolution curve under darkness.

Fig.S23 NH₃ evolution curve under and argon.

Fig.S24 NH₃ production curves of organic monomers.

Fig.S25 Comparison of XRD patterns of TAPT-CHF before and after reaction.

Fig.S26 Comparison of FT-IR of TAPT-CHF before and after reaction.

Fig.S27 The SEM of after reaction.

Fig.S28 The survey XPS spectra of after reaction.

Fig.S29 The C 1s spectra of after reaction.

Fig.S30 The N 1s spectra of after reaction.

Experimental Details

Chemicals and reagents

Melamine ($C_3H_6N_6$, Shanghai Macklin Biochemical Co., Ltd $\geq 99\%$), KOH (Shanghai Macklin Biochemical Co., Ltd $\geq 99\%$), 1,3,5-tris(4-aminophenyl)triazine ($C_{21}H_{24}N_6$, Henan Alpha Chemical Co., Ltd $\geq 98\%$), 1,3,5-tris(4-aminophenyl)benzene ($C_{24}H_{21}N_3$, Henan Alpha Chemical Co., Ltd $\geq 98\%$), Cyanuric chloride ($C_3Cl_3N_3$, Shanghai Macklin Biochemical Co., Ltd $\geq 99\%$).

Materials characterizations

X-ray diffraction (XRD) data were collected on a PC2500 diffractometer. Scanning electron microscope (SEM), energy-dispersive X-ray spectroscopy (EDX, AZtecLive UltimMax100) were observed by Hitachi Regulus 8100. Fourier transform infrared (FT-IR) spectra were acquired on a Thermoscientific Nicolet 4700 Fourier Transform Infrared Spectrometer with KBr pellet. X-ray photoelectron spectroscopy (XPS) was recorded using ESCALAB250X X-ray electron spectrometer (VG Scientific, America). UV-vis diffuse reflectance spectrum (UV-vis DRS) and UV detection were obtained by Cary 500 spectrometer (Shimadzu UV-2550, Japan) and UV-vis spectrophotometer (Shimadzu, UV-2700), respectively. Photoluminescence (PL), time-resolved PL (TR-PL) spectra were characterized by F4500 (Hitachi, Japan) photoluminescence detector and IBH-TemPro (HORIBA JobinYvon, France).

Synthesis of g- C_3N_4

64 g of melamine was placed in an alumina crucible, heated in a muffle furnace at a rate of $5^\circ\text{C}/\text{min}$ to 600°C , and kept for 3 h. After cooling to room temperature, yellow g- C_3N_4 powder was obtained.

Synthesis of $C_6N_7Cl_3$

100 g of KOH, 36 g of g- C_3N_4 , and 700 mL of deionized water were sequentially added to a round-bottom flask and stirred continuously at 160°C in an oil bath for 6 h until fully dissolved. After cooling to room temperature, the solution was transferred to a beaker and stored in the refrigerator overnight. The next day, the resulting sample was filtered, washed, and dried in a vacuum oven at 80°C

for 1 h. After drying, the sample was heated at 180°C for 3 d. The sample was collected, weighed, thoroughly ground with twice its mass of phosphorus pentachloride in a glove box, and placed in a Schlenk tube, then heated at 110°C for 24 h. The product obtained in the oven was not opened, frozen with liquid nitrogen, then poured into ice water, stirred, filtered, and washed with ice water one to two times, minimizing water contact, and freeze-dried at low temperature for 48 h to obtain light yellow C₆N₇Cl₃. Store in a glove box or under other inert gas conditions ^[1-3].

Synthesis of catalyst

The synthesis method of C₆N₇Cl₃ is shown in the supporting information. 100 mg of C₆N₇Cl₃ and 120 mg of 1,3,5-tris(4-aminophenyl)triazine (TAPT)/1,3,5-tris(4-aminophenyl)benzene (TAPB) were added to 20 mL of anhydrous tetrahydrofuran, heated to reflux at 80°C for 24 h, filtered, washed, and dried to obtain powder, which is TAPT-CHF/TAPB-CHF. 100 mg of C₃N₃Cl₃ and 200 mg of 1,3,5-tris(4-aminophenyl)triazine (TAPT) were added to 20 mL of anhydrous tetrahydrofuran, heated to reflux at 80°C for 24 h, filtered, washed, and dried to obtain powder, which is TAPT-CTF.

DFT calculation method

The theoretical calculations were performed via the Gaussian 16 suite of programs ^[4]. The structures of the studied molecules (denoted by M1~M4) were fully optimized at the wB97XD/6-31G(d,p) level of theory. The solvent effect was included in the calculations based on the Polarizable Continuum Model (PCM) using the integral equation formalism variant (IEFPCM). The vibrational frequencies of the optimized structures were carried out at the same level. The structures were characterized as a local energy minimum on the potential energy surface by verifying that all the vibrational frequencies were real. The molecular orbital levels of studied compounds were investigated via theoretical calculations, including the highest occupied molecular orbital (HOMO) and the lowest unoccupied molecular orbital (LUMO). The Visual Molecular Dynamics (VMD) program ^[5] was used to plot the color-filled iso-surface graphs to visualize the molecular orbitals.

Performance measurement

A multi-channel photocatalytic reactor (PCX50C, Beijing Perfectlight, China) was employed for the photocatalytic nitrogen fixation. H_2PtCl_6 (1 wt.% Pt) was employed as a co-catalyst, and 10 mg of the catalyst was uniformly dispersed in a 5 vol% triethanolamine-water solution. Subsequently, nitrogen was continuously added to the solution and stirred in the absence of light for 30 min in order to saturate the reactor with nitrogen adsorption. Subsequently, the mixture was subjected to visible light irradiation (10 W LED, 100 mW cm^{-2} , λ : 400-800 nm). Samples were collected at hourly intervals and the ammonia yield was determined spectrophotometrically using Nessler reagent spectrophotometry.

Results and Discussion

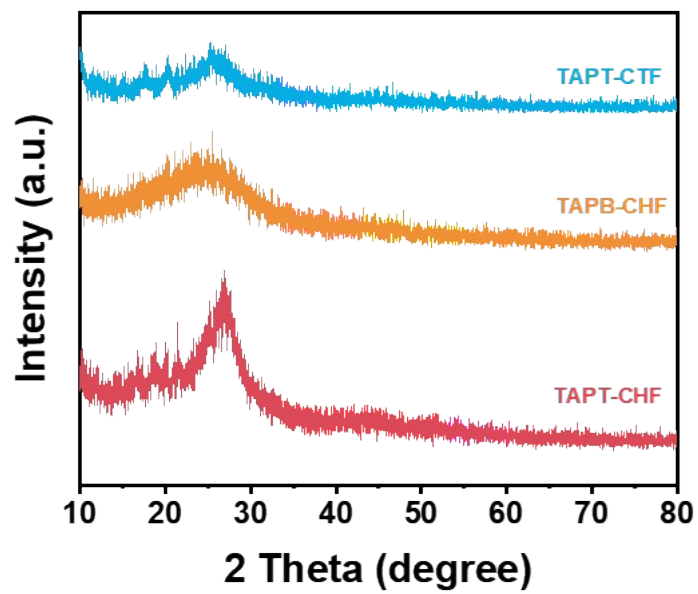


Fig.S1 The XRD of TAPT-CTF, TAPB-CHF, and TAPT-CHF.

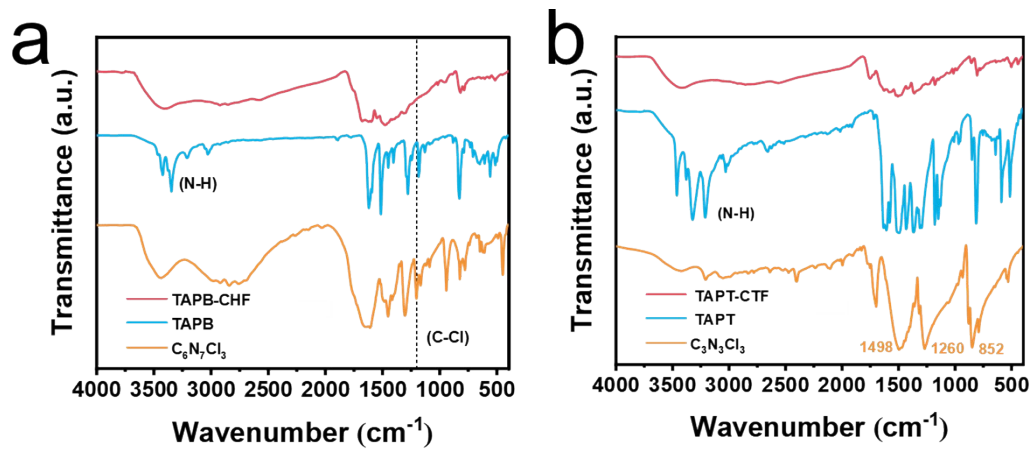


Fig.S2 The FT-IR of TAPB-CHF and TAPT-CTF.

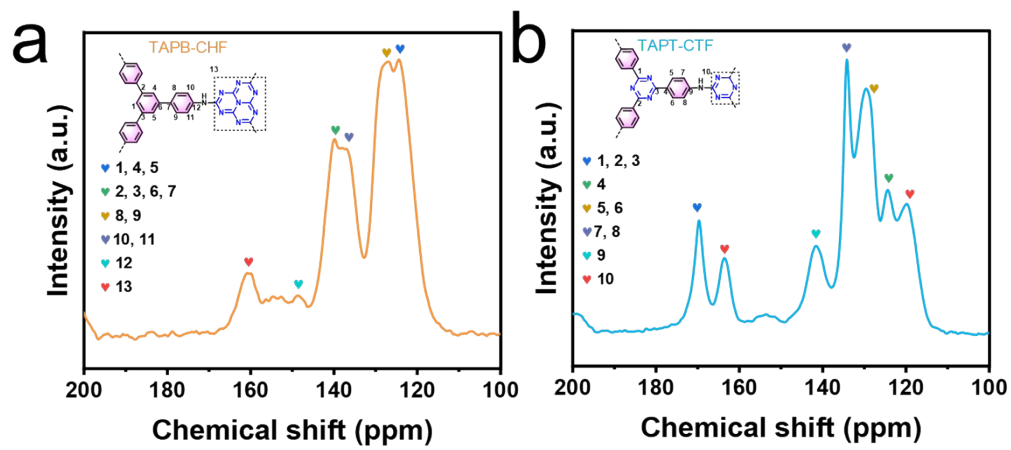


Fig.S3 The ^{13}C NMR of TAPB-CHF and TAPT-CTF.

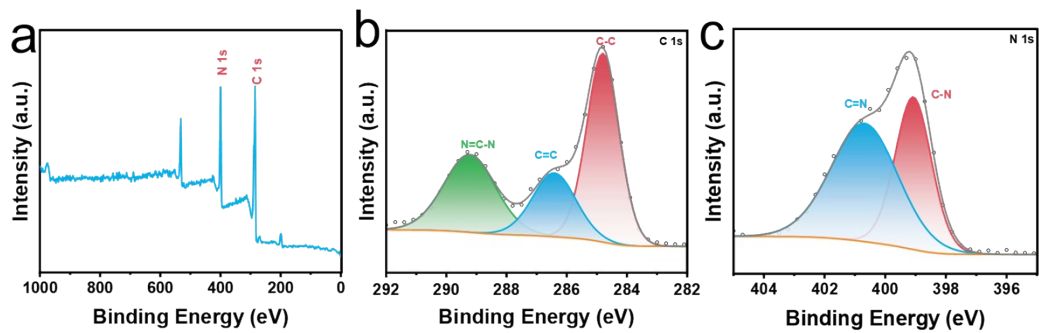


Fig.S4 The (a) survey, (b) C 1s and, (c) N 1s spectra of TAPT-CHF.

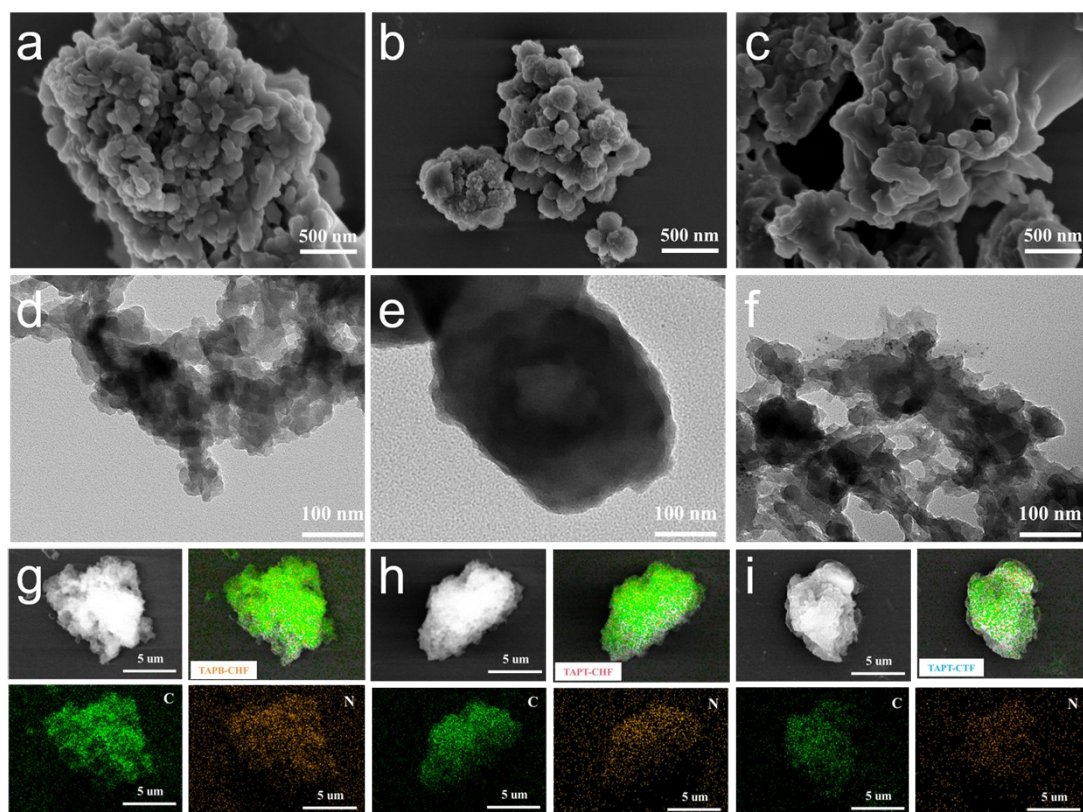


Fig.S5 (a-c) SEM, (d-f) TEM and (g-i) EDS of TAPB-CHF, TAPT-CHF and TAPT-CTF.

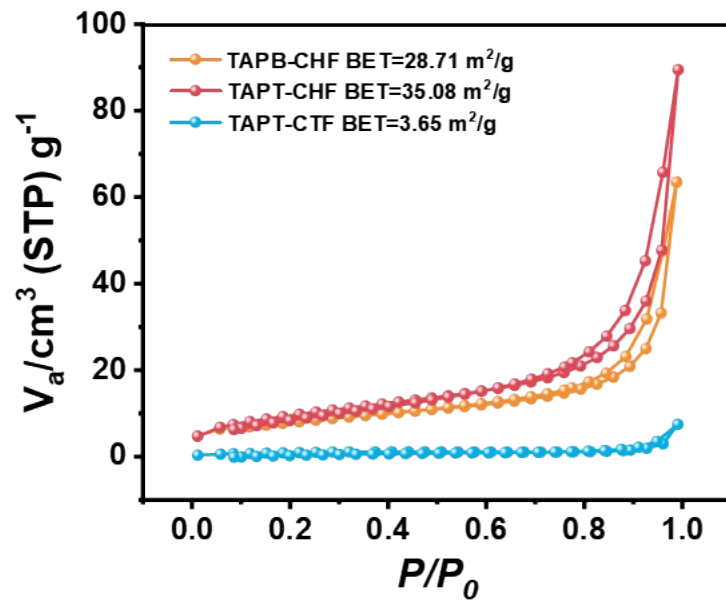


Fig.S6 The N₂ sorption isotherms of TAPT-CTF, TAPB-CHF, and TAPT-CHF.

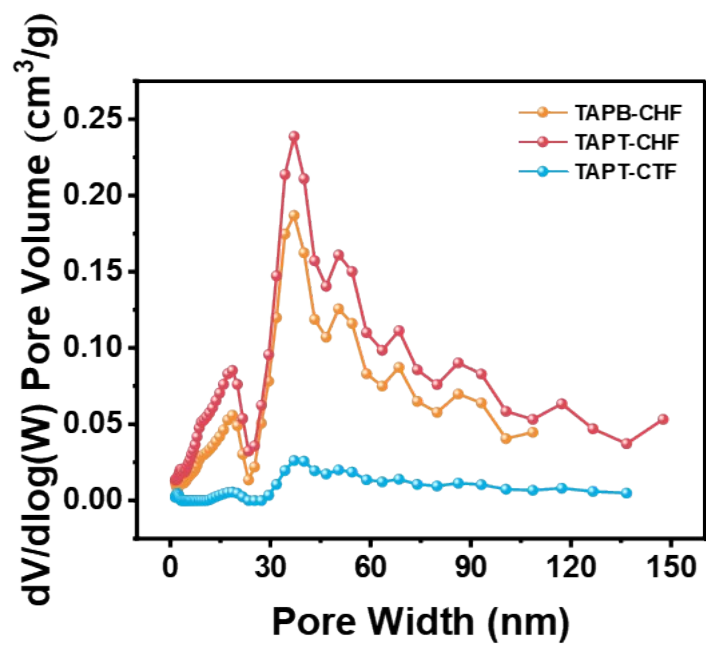


Fig.S7 The pore size distribution curve of TAPT-CTF, TAPB-CHF, and TAPT-CHF.

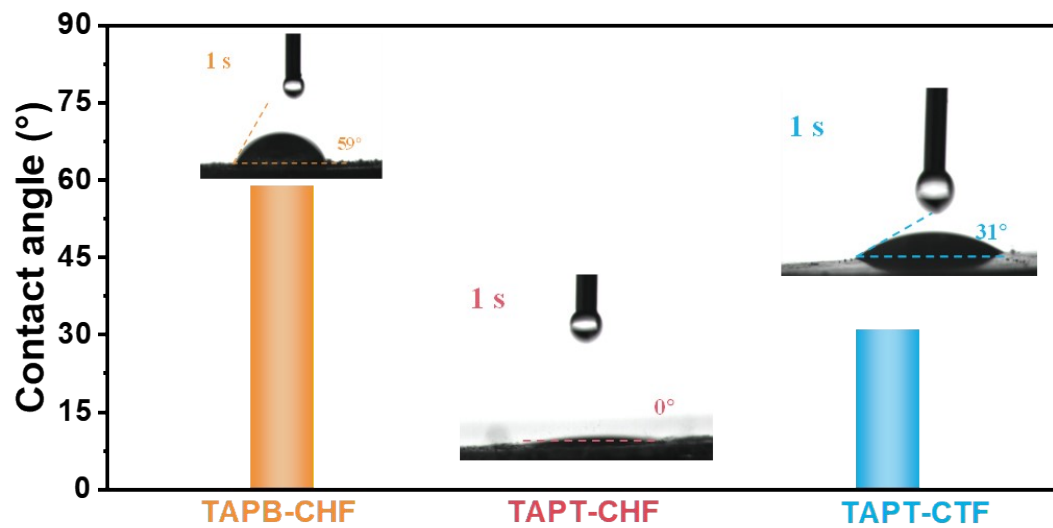


Fig.S8 The contact angle test of TAPT-CTF, TAPB-CHF, and TAPT-CHF.

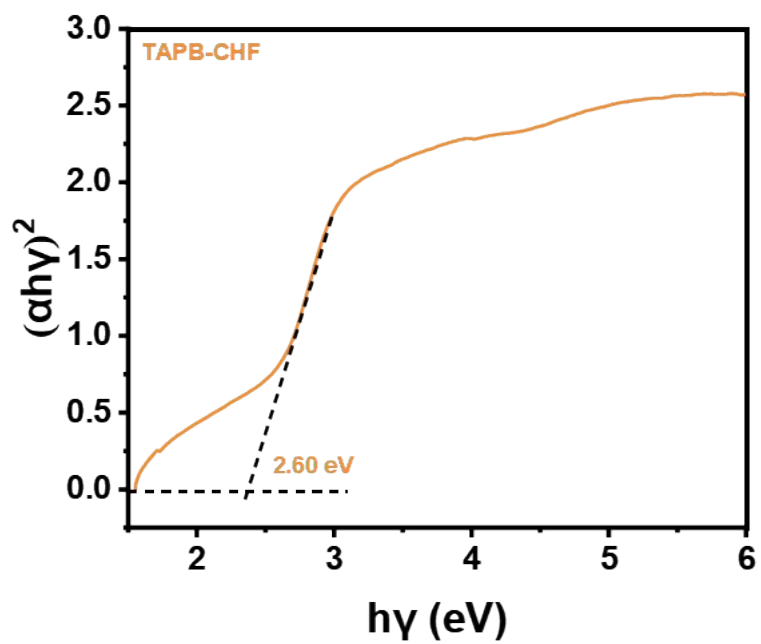


Fig.S9 The bandgap of TAPB-CHF.

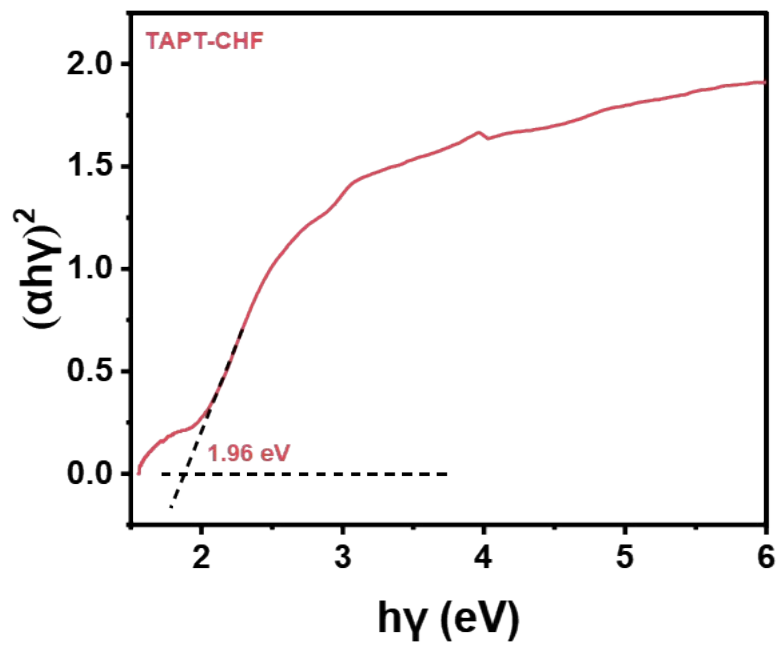


Fig.S10 The bandgap of TAPT-CHF.

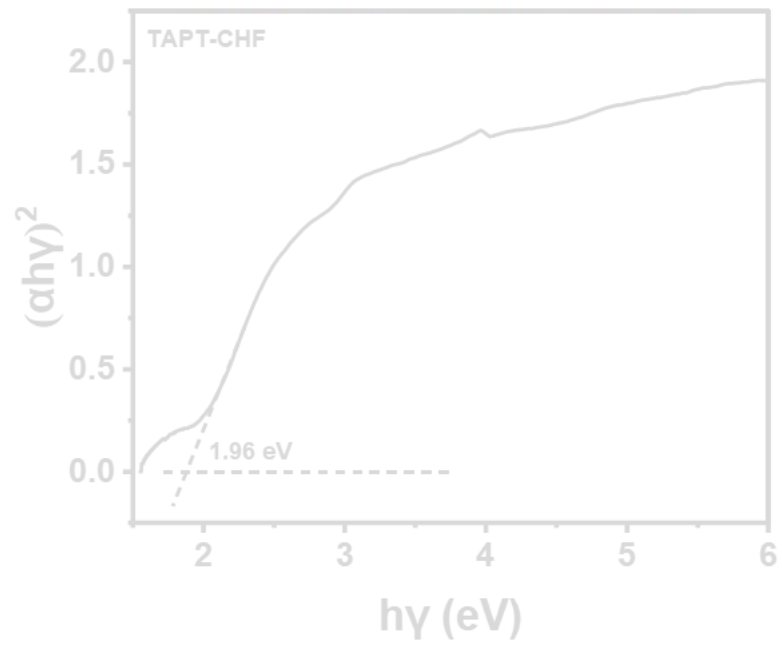


Fig.S11 The bandgap of TAPD-CTF.

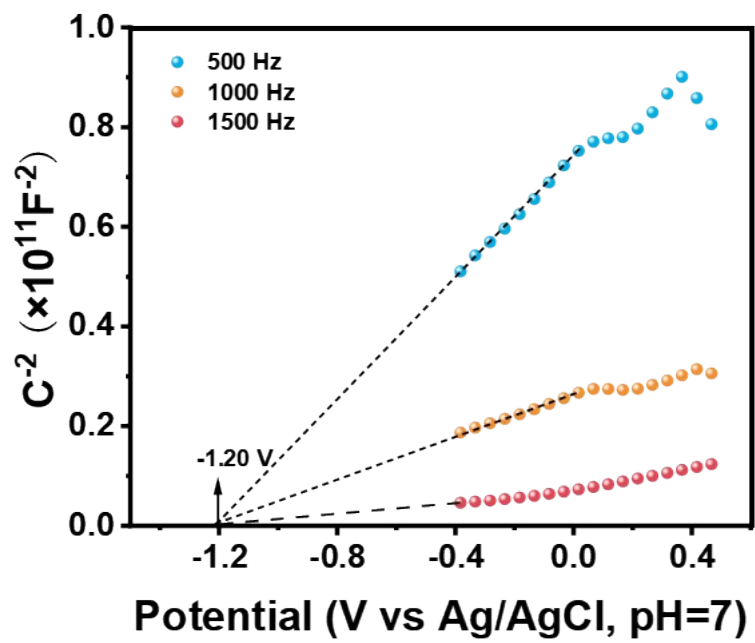


Fig.S12 Mott-Schottky plots of TAPB-CHF.

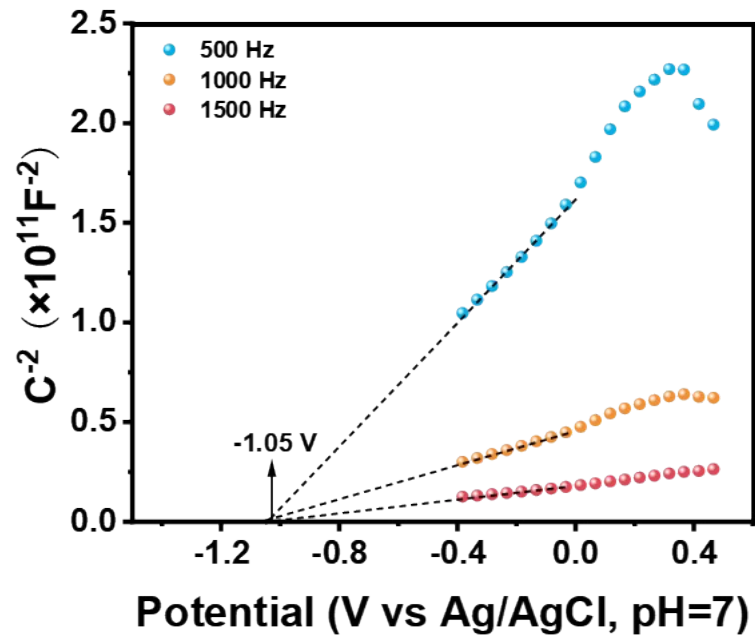


Fig.S13 Mott-Schottky plots of TAPT-CHF.

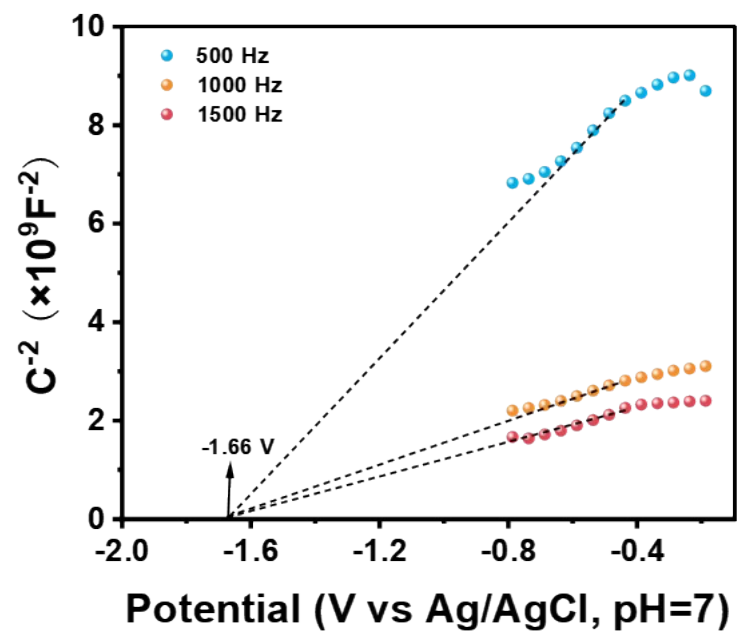


Fig.S14 Mott-Schottky plots of TAPT-CTF.

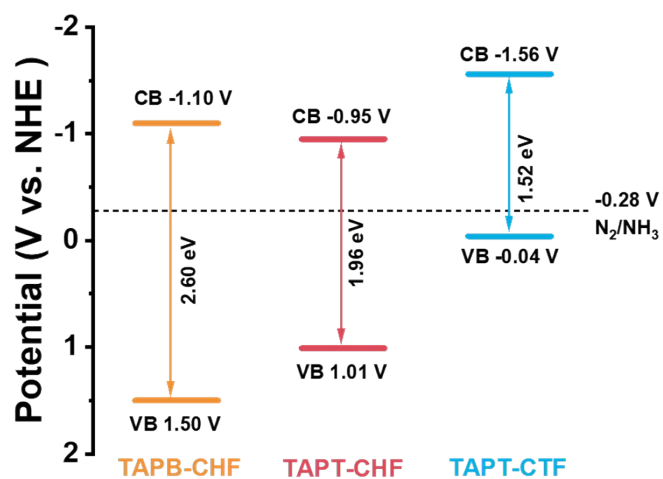


Fig.S15 The band diagram of TAPB-CHF, TAPT-CHF, and TAPT-CTF.

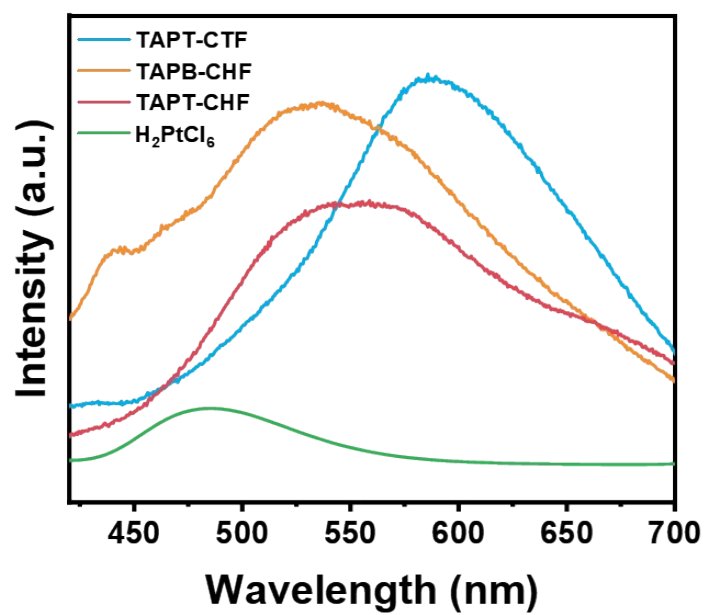


Fig.S16 The PL of TAPB-CHF, TAPT-CHF, TAPT-CTF and H₂PtCl₆.

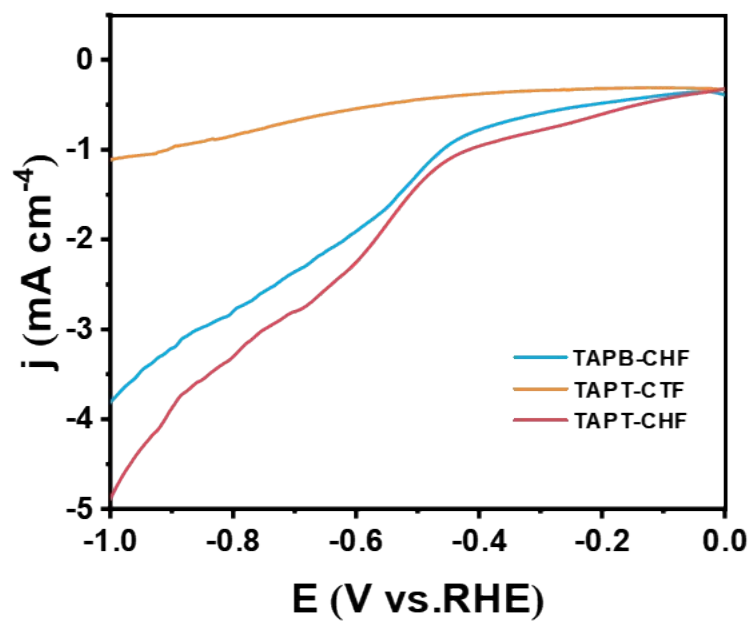


Fig.S17 The LSV of TAPB-CHF, TAPT-CHF and TAPT-CTF.

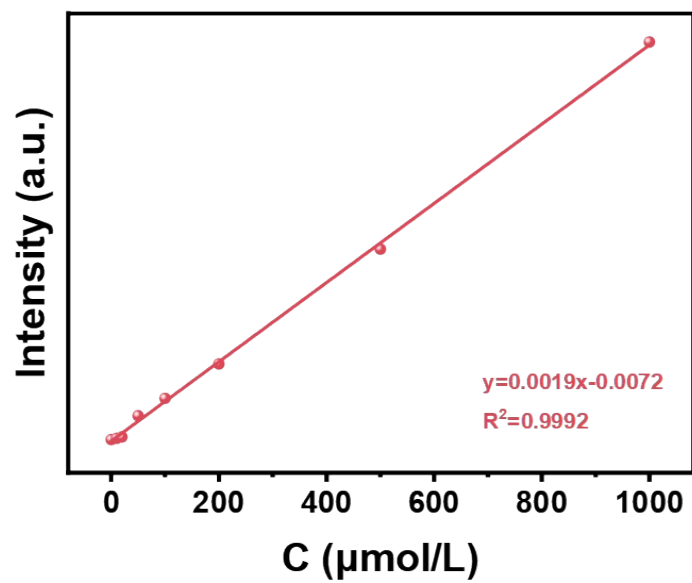


Fig.S18 The standard curve of NH_3 measured by Nessler reagent spectrophotometry.

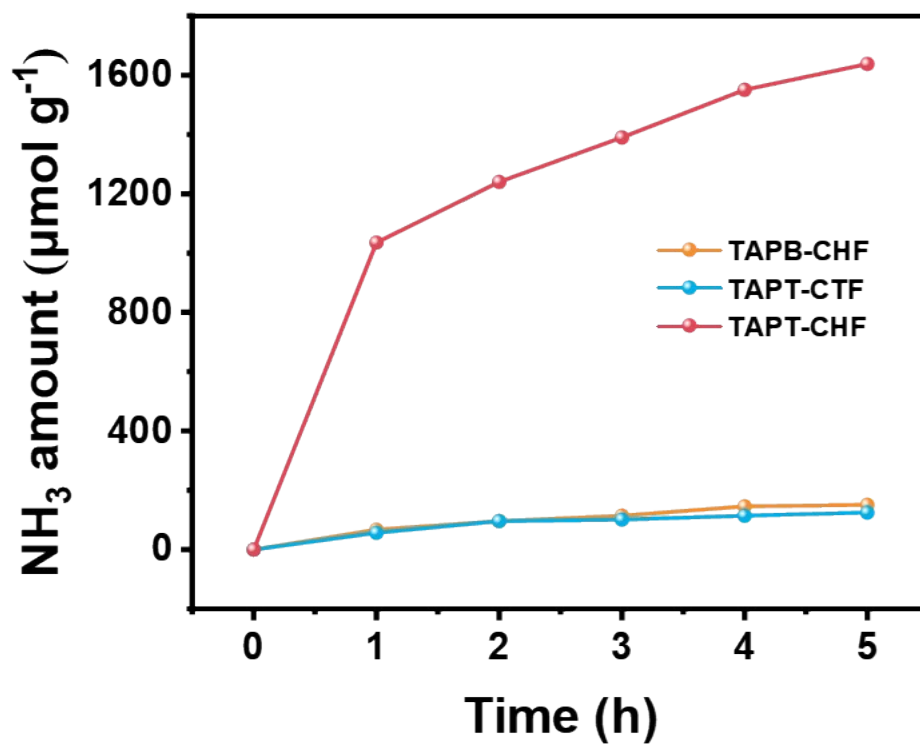


Fig.S19 NH₃ evolution curves.

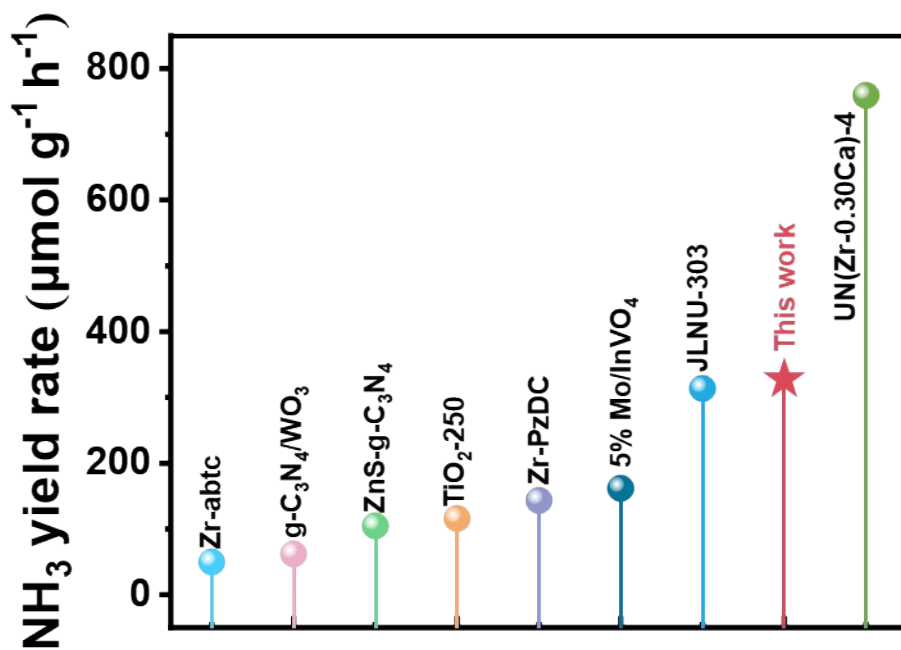


Fig.S20 Comparative analysis among peers.

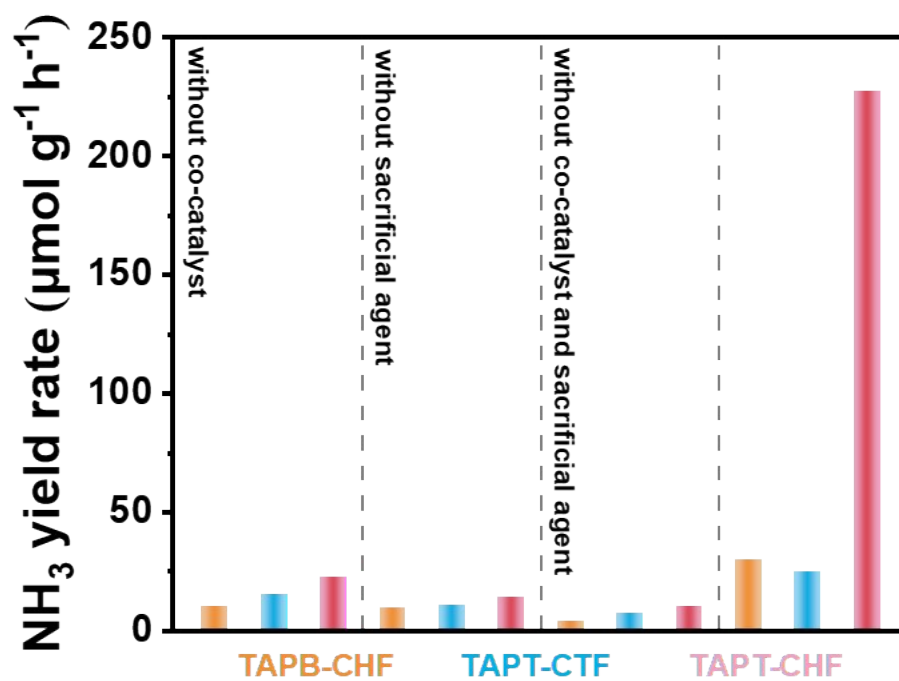


Fig.S21 NH₃ production curves without co-catalyst and sacrificial agent.

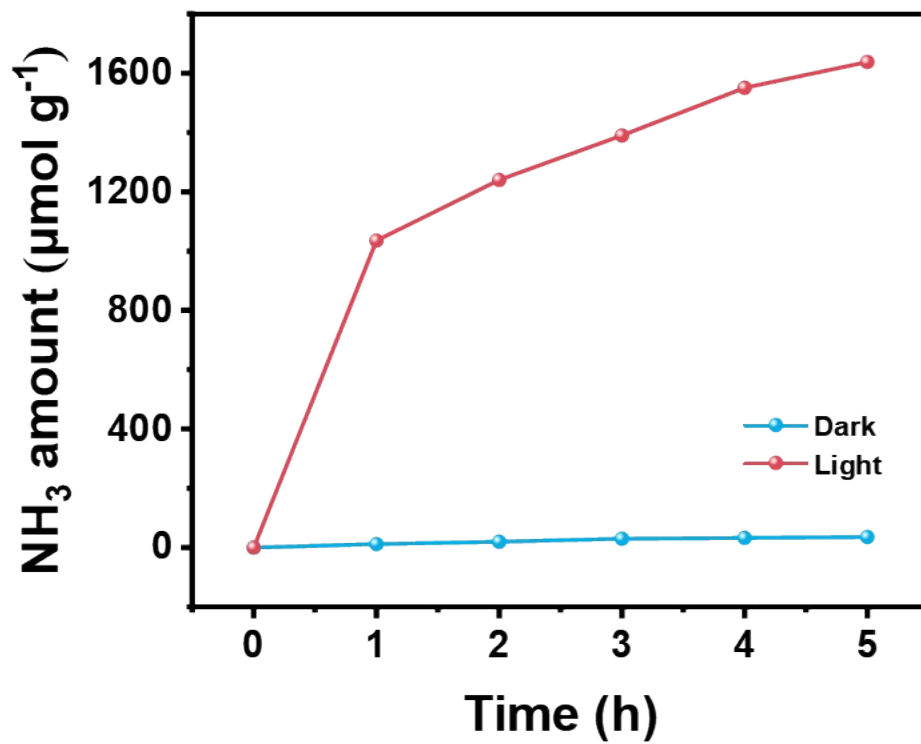


Fig.S22 NH_3 evolution curve under darkness.

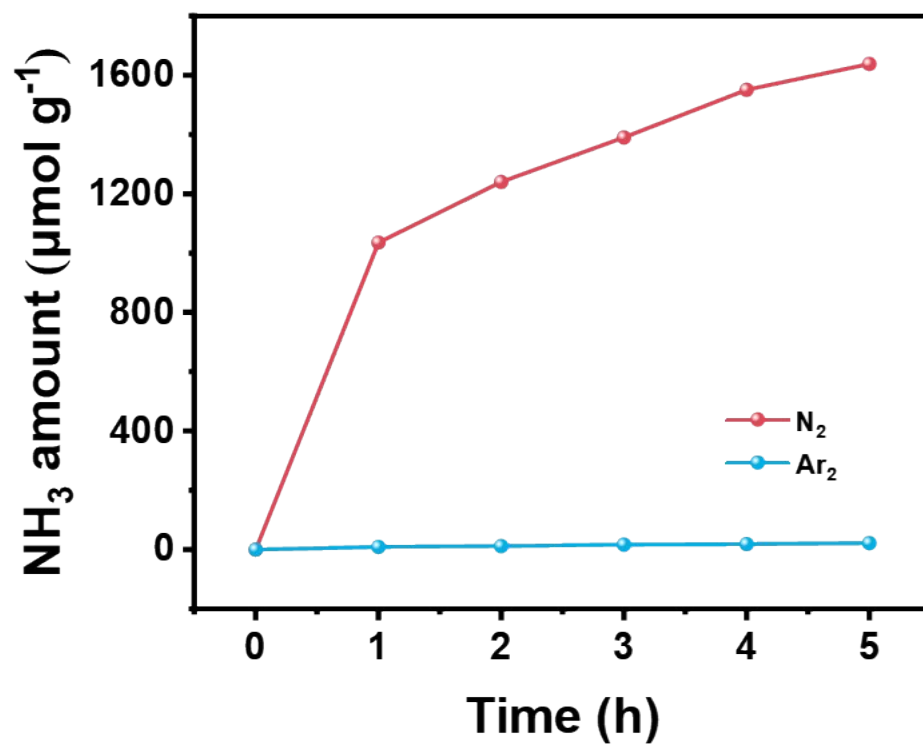


Fig.S23 NH₃ evolution curve under and argon.

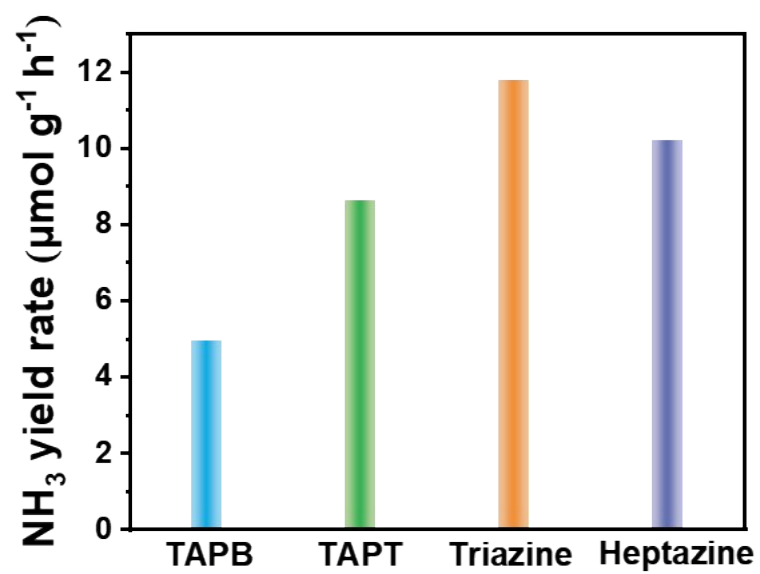


Fig.S24 NH₃ production curves of organic monomers.

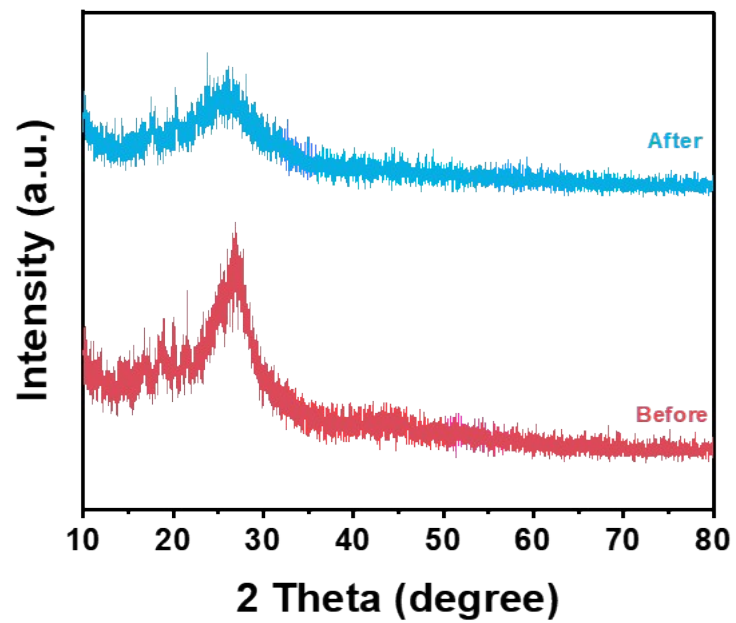


Fig.S25 Comparison of XRD patterns of TAPT-CHF before and after reaction.

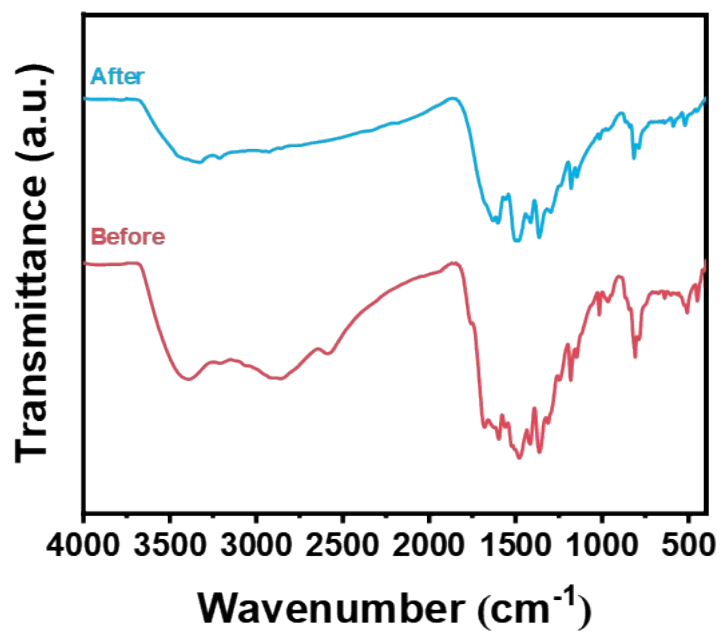


Fig.S26 Comparison of FT-IR of TAPT-CHF before and after reaction.

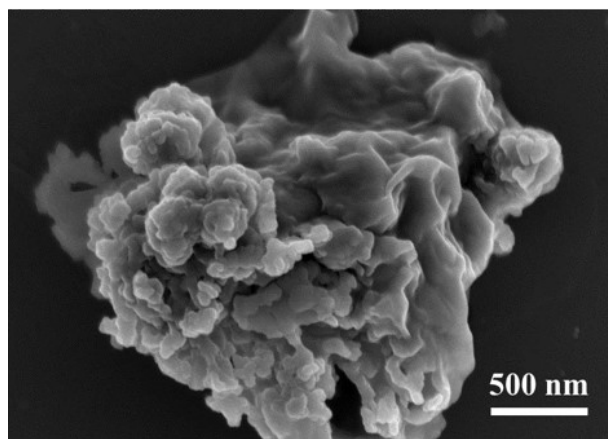


Fig.S27 The SEM of after reaction.

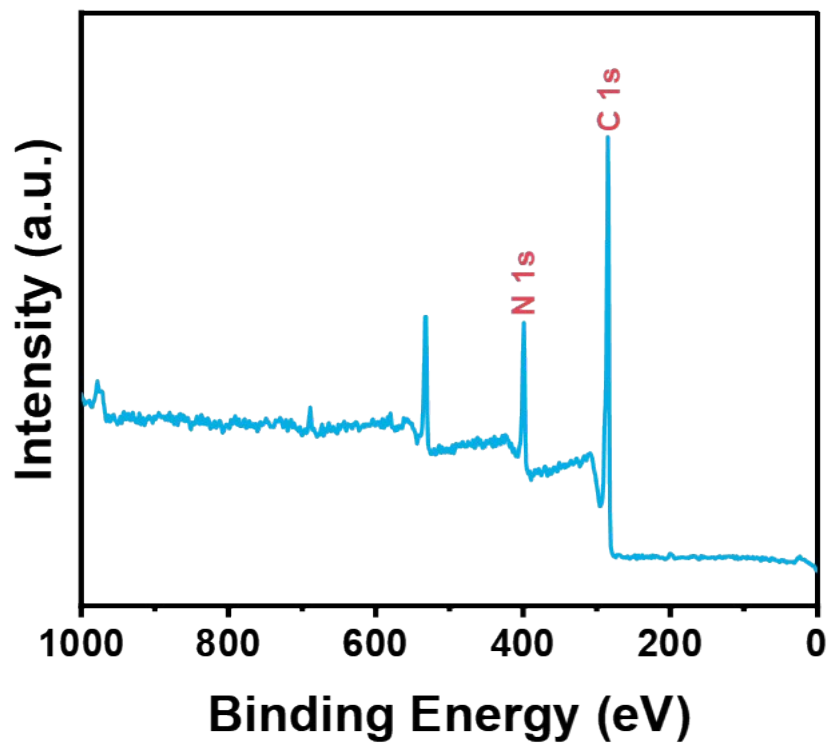


Fig.S28 The survey XPS spectra of after reaction.

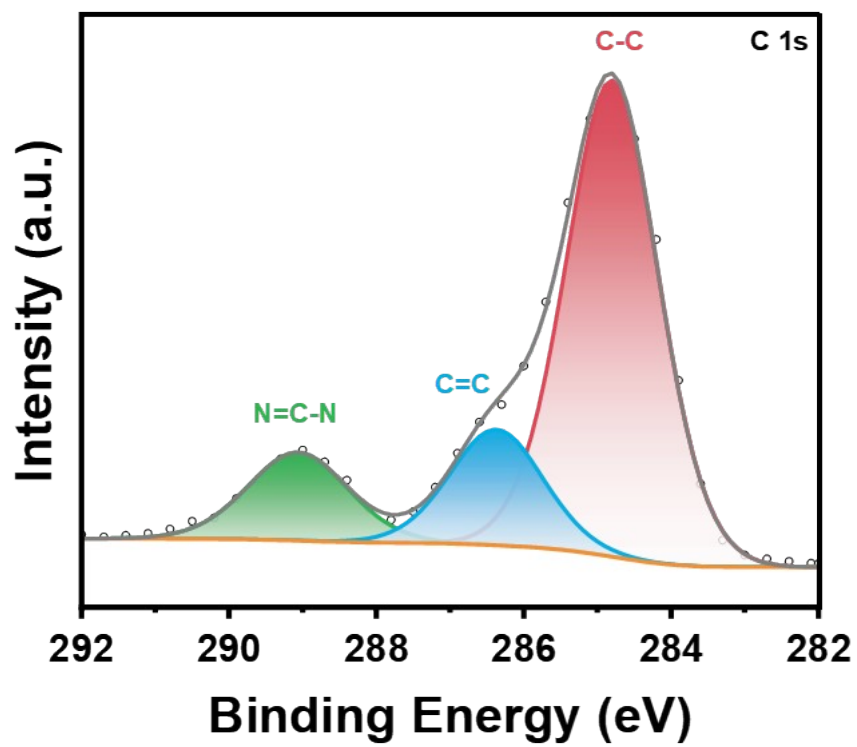


Fig.S29 The C 1s spectra of after reaction.

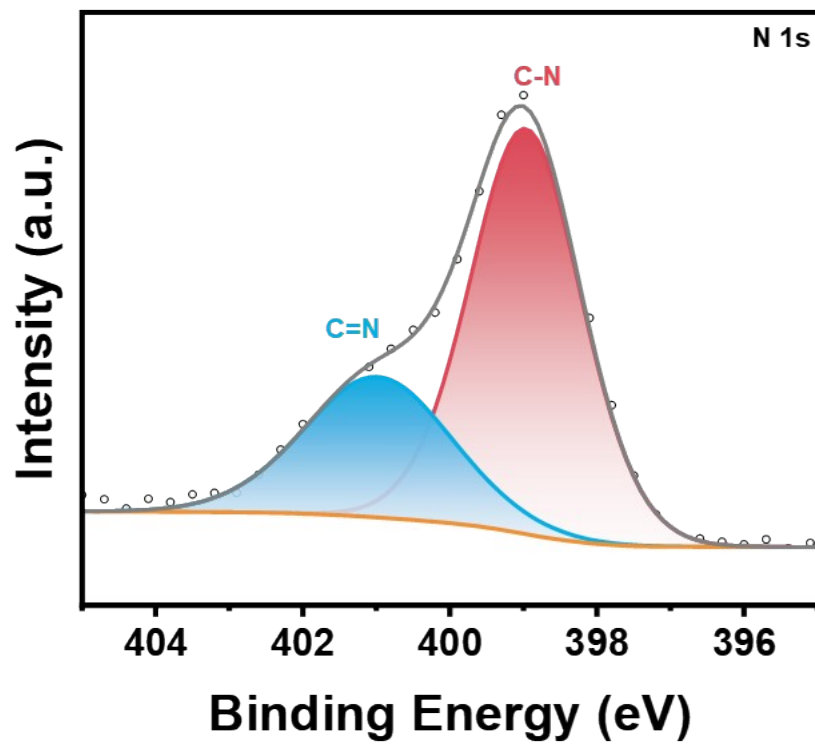


Fig.S30 The N 1s spectra of after reaction.

Table S1 Physicochemical properties of the as-prepared samples.

Samples	S_{BET} ($\text{m}^2 \text{g}^{-1}$)	V_{pore} ($\text{cm}^3 \text{g}^{-1}$)	d_{pore} (nm)
TAPT-CHF	35.0824	0.1384	15.7814
TAPB-CHF	28.7166	0.0983	13.6868
TAPT-CTF	3.6526	0.0115	12.6468

Reference

- [1] H. Cheng, H. Lv, J. Cheng, L. Wang, X. Wu, H. Xu, *Adv. Mater.* **2022**, 34, 2107480.
- [2] X. Wang, C. Wang, H. Tan, T. Qiu, Y. Xing, Q. Shang, Y. Zhao, X. Zhao, Y. Li, *Chem. Eng. J.* **2022**, 431, 134051.
- [3] D. Chen, W. Chen, Y. Wu, L. Wang, X. Wu, H. Xu, *L. Angew. Chem. Int. Ed.* **2022**, e202217479.
- [4] M. J. Frisch, G. W. Trucks, H. B. Schlegel, et al., *Gaussian 16 Revision. A.03*, Gaussian Inc., Wallingford, CT, **2016**.
- [5] W. Humphrey, A. Dalke and K. Schulten, *VMD: Visual molecular dynamics. J Mol Graph Model*, **1996**, 14, 33-38.